Construction and Building Materials 124 (2016) 219–227

Contents lists available at ScienceDirect

Construction and Building Materials

journal homepage: www.elsevier.com/locate/conbuildmat

Use of industrial ceramic sludge in brick production: Effect on aesthetic quality and physical properties

Chiara Coletti [a,b,*], Lara Maritan [a], Giuseppe Cultrone [b], Claudio Mazzoli [a]

[a] Department of Geosciences, University of Padova, Via G. Gradenigo 6, 35131 Padova, Italy
[b] Department of Mineralogy and Petrology, Faculty of Science, University of Granada, Avda. Fuentenueva s/n, 18002 Granada, Spain

HIGHLIGHTS

- Re-using sludge from the ceramic industry as an alternative eco-friendly additive.
- Aesthetic quality and physical properties of traditional bricks and new mix design.
- Economic and ecologic ways of developing bricks from recycled waste.

ARTICLE INFO

Article history:
Received 7 March 2016
Received in revised form 4 July 2016
Accepted 17 July 2016

Keywords:
Bricks
Sludge
Mineralogy
Physical-mechanical properties
Durability
Aesthetic quality
Porosity

ABSTRACT

Most brick companies nowadays focus their research on the recycling of waste, in order to be able to market new types of bricks. In this work, we explored the possibility of using ceramic sludge in brick production, aiming to find an alternative eco-friendly additive to produce "eco-bricks" characterised by suitable mechanical and aesthetic properties and durability. For this purpose, two types of bricks produced by an Italian factory (SanMarco-Terreal) were compared with a newly designed brick obtained from the same starting clay, with the addition of ceramic sludge in place of the traditionally used siliceous sand. Bricks and raw materials were investigated with a multivariate approach, consisting in the mineralogical and chemical analysis, and the final products microstructurally investigated and their physical-mechanical properties determined. Results show that bricks produced with added ceramic sludge can substitute traditional bricks well, fulfilling aesthetic requirements and maintaining sufficient mechanical properties. However, one drawback was that these new materials did not respond to freeze-thaw cycles, highlighting their potential vulnerability in cold climates.

1. Introduction

The raw material used in brick production is mostly composed of clay. The growing demand for high-quality final products, the need to expand company production, and increasing attention to environmental problems (cfr. many regional, national and EC norms) have led to the use of several additives in addition to normal raw clay materials. Additives, both natural and synthetic, act as auxiliary "raw materials" and influence many properties of fired products, such as colour, mechanical strength and durability [1]. In ordinary brick production, quartz-rich sand is the additive mainly used as temper (10–20 wt%) since it is easily available, does not release pollutants at any stage of the production process, reduces plasticity, prevents shrinkage, and improves the mechanical resistance of the finished product.

Several researches have been carried out in the last few decades on creating new types of bricks using additives, often consisting of residual urban and industrial materials [2–9]. These works have often demonstrated the potential of these materials, which have technical advantages and can reduce the environmental impact. The introduction of industrial waste in brick production is also a response to the problem of the disposal of large amounts of waste materials from various industrial activities. Storing these waste materials and the resulting global environmental hazard has increased the demand and development of sustainable alternatives. For these reasons, industrial and academic attention has focused on developing environmentally friendly, low-cost and lightweight construction materials obtained from waste. Bricks mainly consist of clayey materials, can tolerate the addition of waste even in significant percentages, and are therefore suitable for this type of re-use [1].

* Corresponding author at: Department of Geosciences, University of Padova, Via G. Gradenigo 6, 35131 Padova, Italy.
E-mail address: chiara.coletti@studenti.unipd.it (C. Coletti).

http://dx.doi.org/10.1016/j.conbuildmat.2016.07.096
0950-0618/

One type of waste is sludge from ceramic production, consisting mainly of silico-aluminous-based components (>50%), generally with low contents of heavy metals [1]. Being compositionally similar to the raw clayey materials of bricks, this type of waste is related to ceramic production and often inadequately disposed of, although it is an important source of additives in brick production if properly designed new mixes are created. Nowadays, most ceramic-producing companies have addressed their research and organisation of productive plants to recycle waste, save energy and re-use resources (mainly water) deriving from the production cycle, thus saving natural resources and resolving the waste disposal problem. All these aspects contribute much to the evaluation of company performance. Although re-using ceramic production waste (shards) is quite common, re-using sludge is more difficult, due to its intrinsic nature. Sludge is very fine-grained and, according to the type of ceramic production from which it derives, does contain heavy metals in variable quantities, from few ppm as they naturally occur in the base clay and possibly added temper, to some percent, as in the case of glazed and colour ware. Therefore, a sludge does not reflect environmental and human safety requirements, indicating that continual quality control of used materials is always important.

This work explores the possibility of using ceramic sludge in brick production. Two types of commercial bricks produced by the Italian factory SanMarco-Terreal were analysed, and the results were compared with a newly designed brick obtained from the same starting clay tempered with ceramic sludge instead of the traditional siliceous sand. More in detail, the sludge here used was obtained from the mechanical treatment (such as lapping or scrapping) of a clay based highly-fired ceramic material. The mineralogical composition, texture, physical properties, water behaviour and durability of both traditionally produced and newly designed bricks were analysed by a multi-analytical approach, and the possibility of recycling ceramic sludge in brick production was critically evaluated.

This research arose from definite interest on the part of the company, which provided full technical support.

2. Materials and methods

Three types of bricks (two (bricks 1 and 2) commercialized and industrially produced, and one (brick 3) experimentally produced in the SanMarco-Terreal laboratory, simulating the same preparation, forming and firing conditions used for the industrial ones) were prepared with the same carbonate-rich clay, quarried from the area of Marcon (Venice inland) and fired at 1050 °C. Any differences among them were due to the additives used. Bricks were formed by the soft-mud shaping method, in which the clay paste is placed into $5 \times 12 \times 20$ cm moulds, the walls of which are spread with quartz sand to avoid clay from sticking and favour both water drainage while pressing and the separation from the mould. The colour of the commercial bricks was yellow (brick 1) and black (brick 2), and both were prepared by tempering clay with 10 wt% of siliceous sand, but the black brick was obtained adding to the clay paste and quartz sand also 15 wt% of the colouring agent hausmannite ($Mn^{2+}Mn_2^{3+}O_4$). Hausmannite is a secondary waste product, approved according to valid environmental impact criteria [10] and derived from industrial sources, such as the production of ferroalloys and MnO_2-based batteries. The newly designed brick (brick 3) was prepared by tempering the same clay with 10 wt% of dried ceramic sludge provided by SanMarco-Terreal.

Raw materials (clay and sludge) and fired products were chemically analysed by X-ray Fluorescence (XRF) using a S4 Pioneer (Brucker AXS) spectrometer (estimated detection limit for major elements: 0.01 wt%); ZAF correction was performed systematically [11], and the NCSDC 74301 (GSMS-1) standard [12] was applied. Grain-size distribution in the size range between 0.02 and 2000 μm of the sludge was determined using a Mastersizer 2000LF laser diffraction particle size analyser (Malvern Instruments).

The mineralogical composition of raw materials and bricks was determined by X-ray Powder Diffraction (XRPD) on a PANalytical X'Pert diffractometer with Co-Kα radiation, operating at 40 kV and 40 mA intensity; XRPD data were interpreted by X'Pert PRO HighScore Plus® software (PANalytical). Semiquantitative phase analysis was performed on the crystalline phases using the RIR method. Since none internal standard was used during the XRPD acquisition, relative abundance of the amorphous phase was expressed only qualitatively, taking into consideration the pattern profile.

Colour of the raw materials and the fired bricks was determined on a Konica Minolta CM-700d spectrophotometer (10 measures per samples were performed). According to the CIE system, colour is described considering a parameter for luminescence (L^*) and two chromatic coordinates, a^* and b^*, which reflect the amount of red-green (−60: green,+60: red) and yellow-blue (−60: blue,+60: yellow), respectively. Colorimetry was performed in dry and then in wet conditions on the fired bricks, to determine all possible colour changes due to the presence of water or humidity. Colour difference ΔE was calculated according to the following equation:

$$\Delta E = \sqrt{(L_1^* - L_2^*)^2 + (a_1^* - a_2^*)^2 + (b_1^* - b_2^*)^2}$$

where subscript 1 refers to measurements on dry samples and subscript 2 on wet ones.

Petrographic features, texture and degree of vitrification of the bricks were studied on polished thin sections by Optical Microscopy (OM) under polarized light with an Olympus DX–50 equipped with a Nikon D7000 digital microphotography system, and on back-scattered electron (BSE) images obtained by Field Emission Scanning Electron Microscopy (FESEM) with a LEO GEMINI 1530, coupled to an INCA-200 Oxford microanalysis system.

Water absorption [13] and drying [14] tests on fired bricks were performed on cube-shaped samples (50-mm edge) on three samples of each brick type. Free and forced absorption (A_l and A_f), drying index (D_i), apparent and real density (D_a and D_r), open porosity (P) and degree of pore interconnection (A_x) were calculated.

Capillary rise (B) was studied on three prism-shaped samples ($25 \times 25 \times 120$ mm) for each brick type, according to UNI EN 1925 [15]. The coefficient of capillarity (K_s) was calculated 9 min after the test began.

The distribution of pore access size (range 0.003–360 μm) was determined by Mercury Intrusion Porosimetry (MIP) on a model 9410 Micromeritics Autopore apparatus, which can generate a pressure of 414 MPa. Freshly cut samples of approximately 2 cm^3 were oven-dried for 24 h at 110 °C and then analysed. Nitrogen adsorption was used to determine porosity in the range diameter 2–3000 Å. Sorption isotherms were determined at 77 K on a Micromeritics Tristar 3000 in continuous adsorption conditions. Prior to measurement, samples were heated to 130 °C for 24 h and out-gassed to 10^{-3} Torr on a Micromeritics Flowprep. The Barrett-Joyner-Halenda (BJH) method was used to obtain pore-size distribution curves.

V_p (compression pulse) and V_s (shear pulse) propagation velocities were measured to check the elastic-mechanical characteristics and structural anisotropy of the fired bricks, and to detect compactness variations during and after ageing. Waves were transmitted in the three perpendicular directions of the cube-shaped samples (50-mm edge) on a Panametrics HV Pulser/Receiver 5058PR coupled to a Tektronix TDS 3012B oscilloscope.

Measurements were performed with Panametrics transducers of 1 MHz on a contact surface 3 cm in diameter. Once wave velocities (V_p and V_s) and apparent density (by MIP) were established, Poisson's Coefficient (ν), Young (E), shear (S) and bulk (K) modules were calculated.

Uniaxial mechanical tests were carried out on three cubic samples (40 × 40 × 40 mm) on an IPEMSA Model S-110 press with a load force of 20 kg/s, according to UNI EN 1926 [16].

Accelerated ageing tests were carried out on three cubic samples (50 mm edge) for each brick type, to evaluate their resistance to frost and salt crystallisation. Freeze-thaw and salt crystallisation tests followed UNI EN 12371 [17] and UNI EN 12370 [18] norms, respectively. The former consists of 30 cycles each lasting 24 h, each cycle including 8 h of freezing at −12 °C and 16 h of thawing at +20 °C under water. Samples were weighed at each cycle and carefully observed visually to check their progressive decay. At the end of the tests, samples were dried to measure their weight loss. The salt crystallisation test consisted of 10 24-h cycles, during which the samples were immersed for 4 h in a 14 wt% solution of $NaSO_4 \cdot 10H_2O$ at 20 °C, dried for 16 h in an electric oven at 100 °C, and cooled for 4 h at 20 °C. They were weighed at each cycle and observed by visual inspection. They were then washed in water, to remove any salts trapped in pores, and dried to measure their weight loss. During both tests, at regular intervals (every 5 cycles during the freeze-thaw test and every 3 cycles of salt crystallisation), sample compactness was also monitored by ultrasound.

3. Results and discussion

3.1. Clay and recycled materials

According to mineralogical composition (Fig. 1; Table 1), the clay material was an illitic-chloritic highly calcareous (carbonate-rich) clay. The abundance of carbonate was confirmed by the high values of calcium and magnesium oxides, and loss of ignition (Table 2: CaO + MgO = 22.51 wt%; LOI = 19.65 wt%). The abundance of carbonate conferred a yellow hue on the fired bricks, with a high b* value (16.05) (Table 3).

Macroscopically, the powdered sludge was pale yellow in colour, with a high value of lightness (L* = 84.87) and low values of a* and b* coordinates (6.28 and 1.27, respectively) (Table 3). Its grain-size distribution ranged between 0.25 and 1002 μm, with most of the particles (90%) smaller than 100 μm (Fig. 2). Chemically, sludge is highly siliceous, and does not contain heavy metals (Table 1), i.e., it may be used safely in industrial production. From a mineralogical viewpoint, this material is mainly composed of quartz, associated with plagioclase, mullite, cristobalite and an amorphous phase

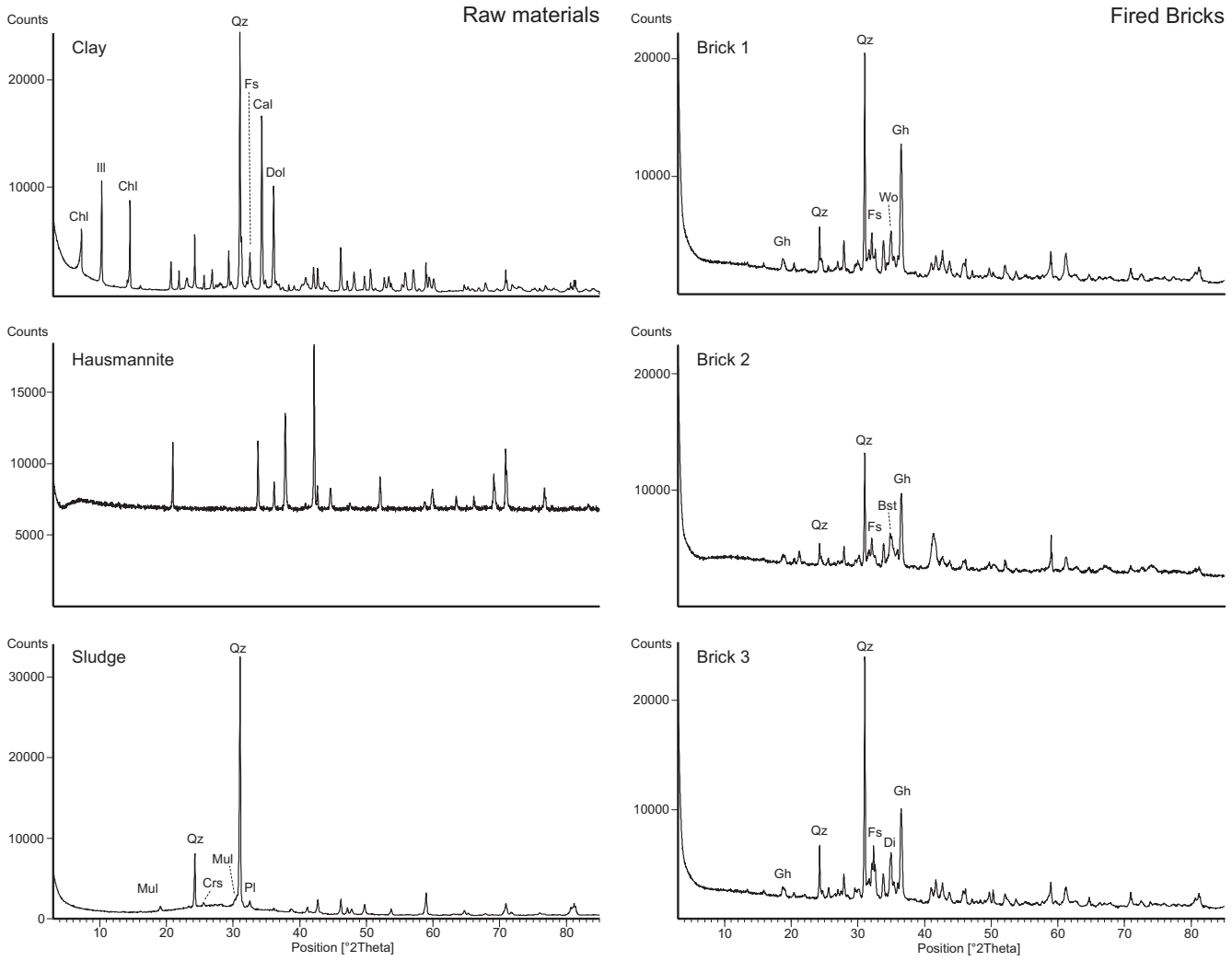

Fig. 1. XRPD patterns of raw materials (clay, hausmannite, sludge) and fired bricks. Hausmannite and Brick 2 show a high background due to the Mn-fluorescence effect in the powder sample produced by the cobalt anode incident radiation.

Table 1
Semi-quantitative mineral composition determined by RIR method on XRPD data of raw clay material, hausmannite (Hsm), sludge and three fired bricks. Mineral abbreviations after Whitney and Evans [40]: Qz = quartz; Ill = illite; Chl = chlorite; Kfs = K-feldspar; Pl = plagioclase; Cal = calcite; Dol = dolomite; Hem = hematite; Hsm = hausmannite; Mul = mullite; Crs = cristobalite; Di = diopside; Gh = gehlenite; Wo = wollastonite; Bst = bustamite. Qualitative estimation of amorphous phase (Am): *** = abundant; ** = - medium; * = scarce; – = absent.

Raw Materials	Qz	Ill	Chl	Kfs	Pl	Cal	Dol	Hem	Hsm	Mul	Crs	Am
Clay	30	12	14	5	6	19	14	1	–	–	–	–
Hsm	–	–	–	–	–	–	–	–	100	–	–	–
Sludge	67	–	–	–	16	–	–	–	–	16	2	**

Fired bricks	Qz	Kfs	Pl	Hem	Wo	Di	Gh	Bst	Am
1	28	11	19	1	12	11	18	–	**
2	21	20	18	1	–	12	16	11	***
3	28	17	21	1	7	13	13	–	*

Table 2
Chemical composition of major elements, expressed in wt% of oxides for clay material and sludge. LOI = Loss on Ignition.

	SiO_2	Al_2O_3	Fe_2O_3	MnO	MgO	CaO	Na_2O	K_2O	TiO_2	P_2O_5	LOI
Clay	39.81	10.63	3.87	0.08	4.75	17.76	0.54	2.37	0.43	0.11	19.65
Sludge	72.52	18.36	1.20	0.01	0.51	1.00	3.11	2.31	0.71	0.11	0.16

Table 3
Colour coordinates L*, a* and b* for raw clay material, hausmannite (Hsm), sludge and three fired bricks, measured in dry and wet conditions. ΔE: colour difference. Concerning the brick with sludge (Brick 3), colour analysis was also performed after salt crystallisation (A.S.C.) test.

	Raw materials					
	L*	SDL*	a*	SDa*	b*	SDb*
Clay	63.89	±1.30	2.41	±0.12	16.05	±1.25
Hsm	35.67	±1.03	10.85	±0.87	8.70	±2.77
Sludge	84.87	±0.27	1.27	±0.03	6.28	±0.22

	Fired bricks												
	Dry						Wet						
	L*	SDL*	a*	SDa*	b*	SDb*	L*	SDL*	a*	SDa*	b*	SDb*	ΔE
Brick 1	71.95	±1.35	6.63	±0.49	23.62	±1.02	58.78	±1.12	9.61	±0.46	26.86	±1.03	13.88
Brick 2	37.05	±0.72	4.48	±0.11	7.32	±0.27	26.22	±0.56	3.72	±0.09	5.30	±0.20	11.04
Brick 3	72.20	±0.77	6.39	±0.56	18.98	±1.00	57.90	±0.55	10.00	±0.41	23.22	±0.80	15.34
Brick 3 A.F.	58.89	±4.02	11.97	±1.52	24.66	±1.99	57.58	±1.03	11.11	±0.31	24.97	±0.55	1.60

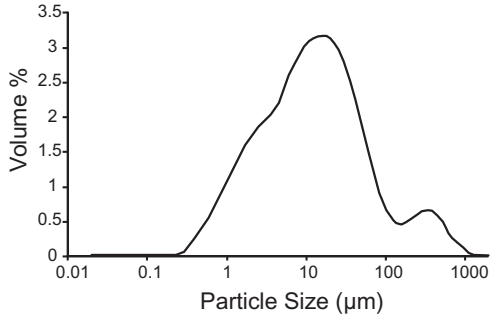

Fig. 2. Grain-size distribution of sludge, expressed as volume percentage.

(Fig. 1; Table 1), indicating that the ceramic material from which the sludge was obtained experienced high firing temperature.

Mullite is a common aluminium silicate found in ceramic products fired at temperatures exceeding 800 °C after kaolinite or illite/muscovite breakdown [19,20]. The presence of amorphous phase also proves the high firing temperature at which the ceramic body underwent partial melting. According to both its chemical and mineralogical composition, sludge used to produce brick 3, did not undergo any further treatment.

The dye added to brick 2 turned out to be mineralogically composed only of hausmannite (Fig. 1; Table 1). It was dark brown in colour, with low values of lightness (L* = 35.67), indicating a tendency to a grey hue, and a* and b* of 10.85 and 8.70, respectively (Table 3).

3.2. Fired bricks

3.2.1. Colorimetry

Fired bricks are all characterised by a fine-grained paste, with a yellow hue for bricks 1 and 3 and a dark grey one for brick 2. Lightness (L*) was far higher for bricks 1 and 3 compared with brick 2; chromatic coordinates a* and b* were very similar in bricks 1 and 3 but higher than those of brick 2 (Table 3). The colorimetric results showed that sludge produces a brick (brick 3) with aesthetic characteristics similar to those obtained with a siliceous sand temper (brick 1).

Changes in L*, a* and b* values were observed when the samples were wetted, although these changes did not affect all the samples in the same way. All bricks became darker with the decrease of the L* parameter.

Bricks 1 and 3 showed a very similar increment in the a* and b* values when wet (Table 3). Colour differences values between dry and wet conditions (ΔE values) are rather similar among all the bricks. Nevertheless, the grey coloured brick (brick 2) recorded the smallest change, while the yellow brick with sludge (brick 3) has the highest variability (Table 3).

3.2.2. Mineralogical composition

The mineral compositions of the bricks followed what was expected from a typical ceramic material made of illitic-chloritic carbonate-rich clay and fired at high temperature (1050 °C).

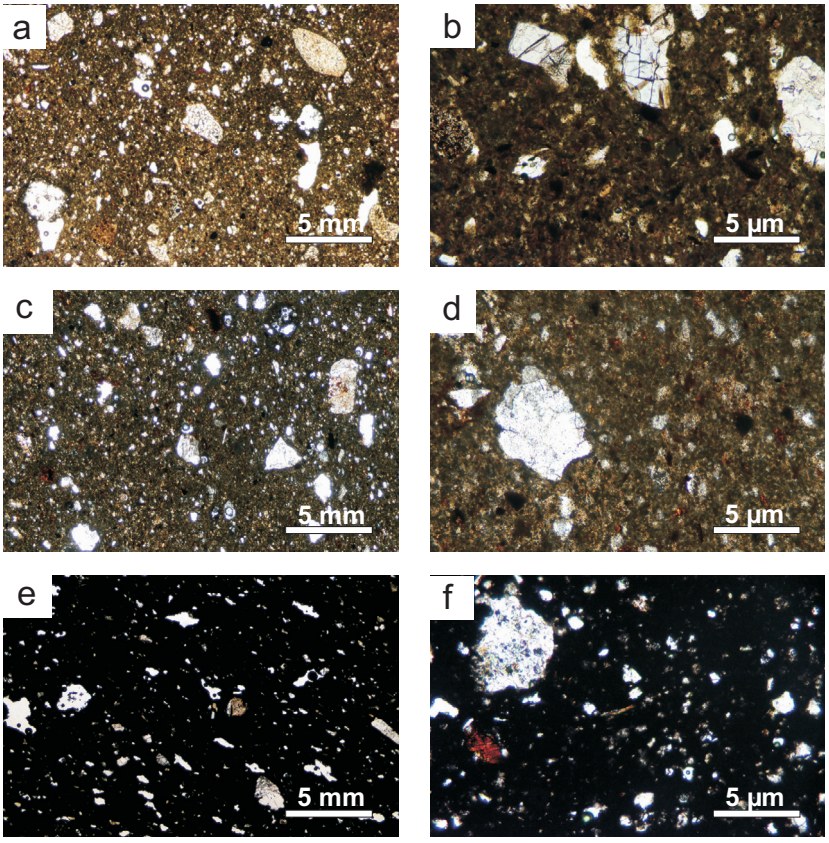

Fig. 3. Photomicrographs (plain polars) of fired bricks: (a, b) brick 1; (c, d) brick 3; (e, f) brick 2.

Brick 1 was composed of predominant quartz, abundant gehlenite, diopside and wollastonite, and associated anorthite, sanidine, hematite and an amorphous phase. It was very similar to brick 2, which also contained bustamite ($CaMnSi_2O_6$), a Mn-rich high-temperature polymorph belonging to the wollastonite group, developed from the following reaction among hausmannite, carbonate and quartz:

$$CaCO_3 + 2SiO_2 + (Mn^{2+}Mn_2^{3+}O_4) \rightarrow CaMn^{2+}Si_2O_6 + Mn_2^{3+}O_3 + CO_2.$$

Brick 3 had the same mineral composition as brick 1, but the newly formed silicates and the amorphous phase were less developed (Fig. 1). The characteristic peaks of mullite, detected in the sludge, were absent in the XRPD diffractogram of the fired product, probably because sludge represented only 10 wt% of the starting raw material, so that its concentration was too low to be detected.

At 1050 °C, most of the minerals composing the clay material and the natural sand had already reacted, causing the disappearance of illite, chlorite and carbonates (calcite and dolomite) [21,22], and contributing to the development of new silicates, such as gehlenite, diopside and wollastonite (or bustamite). Decarbonation of calcite takes place at 750–850 °C and plays an important role in the development of new phases, due to the release and migration of Ca^{2+} cations, promoting reactions between minerals in the matrix. Gehlenite, for example, may derive from calcite and illite (at 800–850 °C), and wollastonite can grow by reaction between calcite and quartz (at 900–1000 °C) [23,24]. When dolomite decarbonates between 700 °C and 800 °C, Mg^{2+} and Ca^{2+} cations are released, their reaction with quartz or silica derived from the decomposition of clay minerals gives rise to the formation of diopside at 900–1050 °C [25]. Orthoclase, initially present in the raw clay, is transformed into its high-temperature polymorph sanidine [25]; plagioclase is enriched in anorthite over 950 °C [23].

3.2.3. Texture

Under the optical microscope, bricks 1 (Fig. 3a, b) and 3 (Fig. 3c, d) had a bright matrix (groundmass), whereas brick 2 (Fig. 3e, f) had a dark groundmass, due to bustamite. All samples were very similar in terms of pore structure and grain-size distribution. Grains (about 20%) were sub-angular in shape, with non-selected distribution. Pores were mainly represented by "vesicles" and "vughs" [26] and were homogeneously distributed in the matrix.

Reaction microstructures were better analysed by scanning electron microscope. The decomposition of carbonates and the migration of Ca^{2+} cations led to development of the sub-solidus reaction with silicates and the growth of new mineral phases.

In brick 1, feldspar and quartz grains showed reaction rims, with a corona-like structure, composed of gehlenite and wollastonite (Fig. 4a). Micro-chemical analysis indicated a progressive increase in Ca from core to rim, as also shown in Fig. 4b, in which the corona structure forming round a grain of quartz displays various grey hues. In this case, wollastonite ($CaSiO_3$) formed by reaction of carbonate in contact with the quartz grain:

$$CaCO_3 + SiO_2 \rightarrow CaSiO_3 + CO_2.$$

Brick 2 was characterised by the diffuse presence of bustamite grains, randomly distributed in the matrix and at feldspar and quartz rims, also identified by XRPD analysis, abundant secondary vesicles (Fig. 4c), and a high level of bonding between matrix and grains. In this brick, hausmannite promoted melting. It was interesting to note that phyllosilicates, which underwent complete dehydroxylation but maintained their sheet-like texture, were here enriched in Mn derived from hausmannite decomposition (Fig. 4d). Secondary rounded pores and vesicles were also seen in brick 3 (Fig. 4e), as well as fibrous Mn-enriched wollastonite crystals at quartz-grain rims (Fig. 4f).

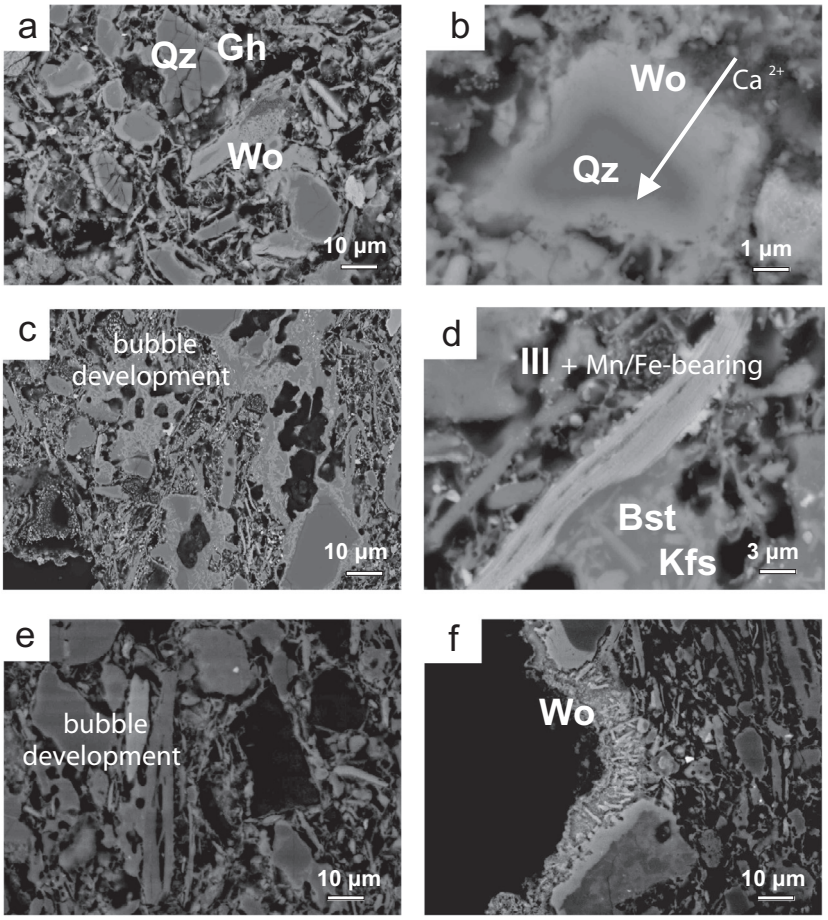

Fig. 4. FESEM-BSE images: (a) quartz and feldspar grains with reaction rims where gehlenite and wollastonite formed (brick 1); (b) Ca^{2+} enrichment at quartz rim with sub-solidus reaction producing wollastonite (brick 1); (c) diffuse occurrence of bustamite ($CaMnSi_2O_6$) and considerable development of rounded pores forming bubbles by reaction among minerals in groundmass (brick 2); (d) K-feldspar with formation of bustamite and phyllosilicate (Ill), with abundant Fe- and Mn-bearing oxides (brick 2); (e) development of bubble-shaped pores and reaction rims (brick 3); (f) fibrous wollastonite crystals growing on quartz grains close to pores (brick 3). Abbreviations as in caption of Table 1.

Table 4
Hydric parameters: A_b = free water absorption (%); A_f = forced water absorption (%); A_x = degree of pore interconnection (%); D_i = drying index; p_{oHT} = open porosity (%); D_{bHT} = apparent density (kg m^{-3}); D_{skHT} = real skeletal density (kg m^{-3}); K_s = capillarity coefficient (g cm^{-2} min$^{-½}$); B = capillarity rise (cm min$^{-½}$). MIP values: p_{oMIP} = open porosity (%); D_{bMIP} = apparent density (kg m^{-3}); D_{skMIP} = real (skeletal) density (kg m^{-3}). N_2 adsorption: BHJ des. V. = BHJ desorption Volume (cm^3 g^{-1}).

		1	DS1	2	DS2	3	DS3
Hydric test	Free water absorption (A_b)	27.63	±0.57	25.08	±0.61	27.94	±0.36
	Forced water absorption (A_f)	28.71	±0.83	25.85	±0.64	28.34	±0.25
	Degree of pore interconnection (A_x)	3.76	±1.20	2.98	±0.20	1.43	±0.42
	Drying index (D_i)	1.35	±0.00	1.36	±0.00	0.39	±0.00
	Open porosity (p_{oHT})	41.36	±1.00	40.56	±0.75	42.12	±0.30
	Apparent density (d_{bHT})	1.44	±0.01	1.57	±0.01	1.49	±0.00
	Real skeletal density (d_{skHT})	2.46	±0.03	2.64	±0.02	2.57	±0.01
	Capillarity coefficient (K_s)	0.43	±0.04	0.33	±0.07	0.41	±0.04
	Capillarity rise (B)	1.33	±0.03	1.23	±0.12	1.05	±0.07
MIP	Open porosity (p_{oMIP})	47.45	–	46.87	–	49.57	–
	Apparent density (d_{bMIP})	1.40	–	1.50	–	1.60	–
	Real (skeletal) density (d_{skMIP})	2.68	–	2.87	–	3.10	–
N_2 ads	BHJ desorption Volume (BJH des.V.)	0.004450	–	0.009709	–	0.001566	–

3.2.4. Hydric behaviour and porosity

The hydric parameters (Table 4) indicated that the three bricks differed in their water behaviour. Brick 3 was the sample with the highest free absorption value (A_b = 27.94%) and the best pore interconnections (A_x = 1.43%), indicating pores favouring water access. Brick 1 was the sample with the greatest difference between free and forced absorption (A_b = 27.63%; A_f = 28.71%), as confirmed by the highest A_x value (3.76%), suggesting the difficulty of water migrating within the brick. Brick 2 showed intermediate characteristics.

Drying was very similar for bricks 1 and 2 (D_i values: 1.35 and 1.36, respectively), although brick 3 dried faster (D_i = 0.39). Open porosity p_0 was quite similar in all samples, the highest value being recorded in brick 3 (p_0 = 42.12%) and the lowest in brick 2

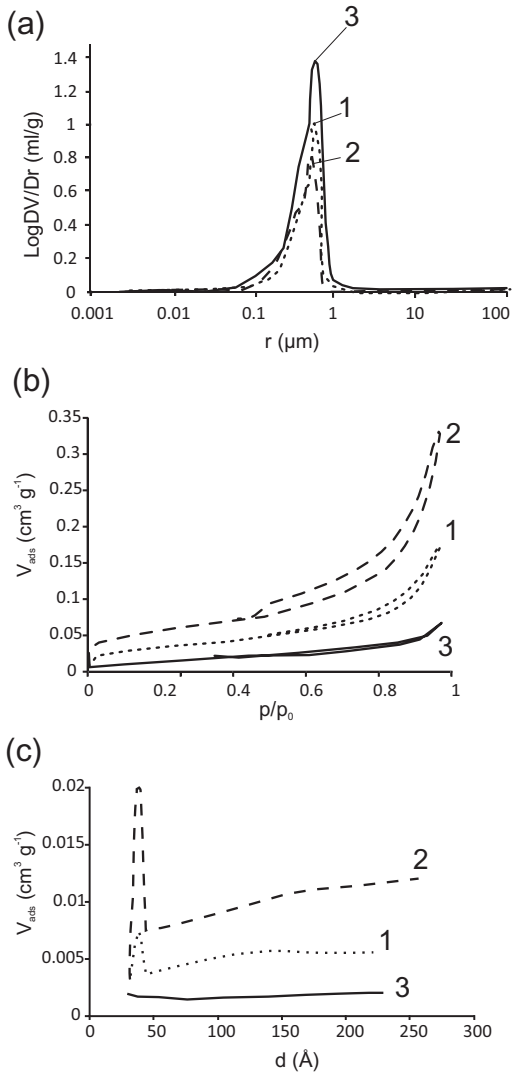

Fig. 5. (a) Pore size distribution curves (log differential intruded volume (ml g^{-1})) vs. pore radius (μm) of all bricks; (b) N_2 isotherms of all bricks: volume adsorbed (cm^3 g^{-1}) vs. differential pressure (p/p$_o$); (c) cumulative curves by BHJ method of all bricks: volume adsorbed (cm^3 g^{-1}) vs. pore diameters (Å).

(p_0 = 40.56%). Brick 1 showed the highest attitude to capillarity rise (K_s = 0.43), followed by brick 3 (K_s = 0.41) and brick 2 (K_s = 0.33).

All samples were characterised by similar porosimetric curves, with predominant pore radius around 1 μm, and differences in the height of the main peak depending on porosity access to mercury (Fig. 5a). Open porosity obtained by MIP was always higher than that measured by water absorption, but followed the same trend, brick 3 showing the highest open porosity (p_0 = 49.5%), followed by brick 1 (p_0 = 47.45%), and brick 2 (p_0 = 46.87%) (Table 4).

Analysis of pores smaller than 0.03 μm in diameter by nitrogen adsorption indicated that brick 3, characterised by the highest open porosity, was the sample which contained fewer micropores (Fig. 5b). Instead, brick 2, with the lowest values of open porosity, showed adsorption-desorption isotherms with the highest values, indicating the greatest number of micropores.

All samples, according to the IUPAC classification, had nitrogen sorption isotherms type IV with H3 hysteresis loop [27,28], typical of mesoporous materials. This phenomenon was particularly evident in brick 2, which also had the greatest amount of gas volume intruded. BJH pore-size distribution for bricks 1 and 2 showed a peak between 30 and 50 Å, indicating the occurrence of small pores

Table 5
Ultrasonic test. Propagation velocities of ultrasonic Vp and Vs pulses (m s^{-1}). ΔM = total anisotropy (%); ν = Poisson's ratio; E = Young's modulus (GPa); G = shear modulus (GPa); K = bulk modulus (GPa). Uniaxial test: σ = stress values (N mm^{-2}).

	1	DS1	2	DS2	3	DS3
Compression pulse (Vp)	2773	±94	2804	±75	2423	±150
Shear pulse (Vs)	1299	±71	1299	±50	1326	±100
Total anisotropy (ΔM)	12.26	±4.88	10.73	±1.24	12.30	±4.86
Poisson's ratio (ν)	0.36	±0.01	0.37	±0.00	0.29	±0.01
Young's modulus (E)	64	±3	63	±3	72	±3
Shear modulus (G)	11	±2	12	±1	15	±1
Bulk modulus (K)	76	±6	79	±7	57	±4
Stress values (σ)	14.80	±1.66	18.73	±2.55	15.20	±2.74

in this pore-size interval (Fig. 5c). Conversely, the absence of these micropores was the main cause, together with the best pore interconnections, of the faster drying velocities of brick 3 [19]. This evidence indicates that the addition of sludge, probably because of its grain size and high degree of vitrification, determines lower microporosity than the other two bricks; instead, the addition of manganese oxide is responsible for increases in microporosity.

3.2.5. Physical-mechanical properties and durability

The highest average value of propagation velocities of brick 2 (Vp = 2773 m s^{-1}) (Table 5) was due to its high amorphous phase, which increased its compactness and made it more homogeneous. This sample was in fact the brick with the lowest total anisotropy (ΔM = 10.73%) [19,29]. Bricks 1 and 3 showed very similar anisotropy, although slightly higher (ΔM = 12.26% and 12.30%, respectively), and the latter the lowest propagation velocity (Vp = 2423 m s^{-1}) due to its higher porosity, as attested by hydric tests and MIP.

Brick 2 also had the highest values of Poisson's ratio (ν = 0.37 GPa) and bulk modulus (K = 79 GPa), followed by bricks 1 (ν = 0.36, K = 76 GPa) and 3 (ν = 0.28, K = 56 GPa). The latter clearly had the highest values for Young (E = 72 GPa) and shear (G = 15 GPa) modules (Table 5), indicating that brick 2 was stiffer, but brick 3 was softer.

Compressive strength values (σ) measured with the uniaxial compressive test confirmed almost all the results obtained by ultrasound, the highest σ value being measured on brick 2 (σ = 18.73 N mm^{-2}), followed by bricks 1 and 3, which showed very similar resistances (σ = 14.80 N mm^{-2} and 15.20 N mm^{-2}, respectively). The apparent discordance of these two samples, between bulk modulus (K) obtained by ultrasound and the compressive test (σ), was due to the higher porosity of brick 3 (according to both hydric tests and MIP) which decreases the capacity of wave transmission during ultrasound tests.

Subjected to ageing tests, the three bricks showed different behaviour. Although they behaved similarly during the first cycles, brick 3 started to fall apart after cycle 18 of the freeze-thaw test, with a consequent loss of fragments and weight (Fig. 6a) and a decrease in ultrasonic wave transmissions (Fig. 6b). From cycle 20 onwards, ultrasonic waves could not be measured in this brick, which suffered progressive decay until its total disintegration after cycle 30, with a weight loss of 95.62%. The behaviour of the other two bricks was very different, weight losses being 3.50% in brick 1 and 0.30% in brick 2 after cycle 30 (Table 6).

The behaviour of samples submitted to salt crystallisation was very different to that after the freeze-thaw cycles. Bricks 1 and 2 showed damaged edges at the end of the test, whereas brick 3 appeared to remain almost intact. Weight variations during the test confirmed these different behaviours. Bricks 1 and 2 increased their weight initially, due to crystallisation of salt in the pores; they then maintained an oscillating trend caused by salt crystallisation within the pores and fissuring, with loss of fragments. At the

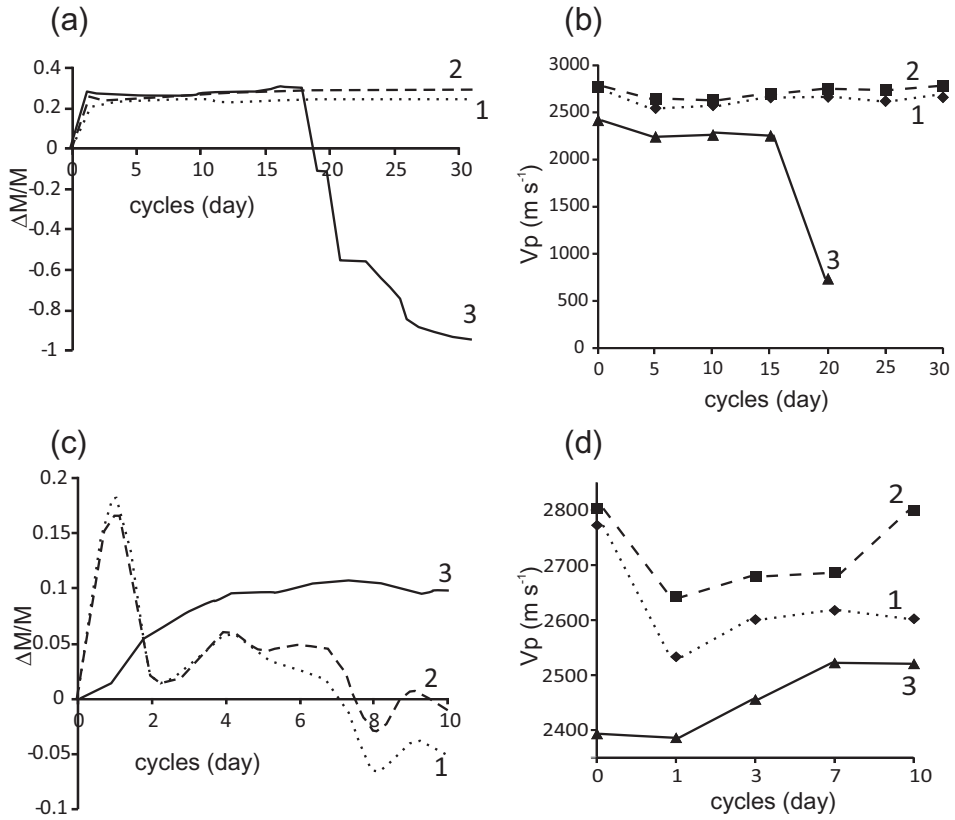

Fig. 6. (a) Weight variation (ΔM/M) vs. cycles (days) of all bricks subjected to 30 freeze-thaw cycles; (b) propagation velocities of ultrasonic Vp pulses (m s^{-1}) during freeze-thaw tests; (c) weight variation (ΔM/M) vs. time (h) of bricks subjected to 10 salt crystallisation cycles; (d) propagation velocities of ultrasonic Vp pulses (m s^{-1}) during salt crystallisation tests.

Table 6
Weight loss $(W_f - W_i)/W_i$ of dried samples after 10 cycles of salt crystallisation test and 30 cycles of freeze-thaw test.

	1	2	3
Salt crystallisation test	−14.28	−10.40	1.05
Freeze-Thaw test	−3.50	−0.30	−95.62

end of the tests, they had lost up to 15% (brick 1) or 10% (brick 2) of their weight (Fig. 6c). Instead, brick 3 showed a gradual weight increase until the last cycle, due to constant accumulation of salt inside the pore system. This was also confirmed by ultrasound, which showed a gradual increase in Vp values (Fig. 6d). At the end of the test, brick 3 recorded the lowest variation in weight, with a small increase of ≈ 1% (Table 6) due to residual salt trapped in the pores after washing. The performance of the other two bricks was clearly worse, with weight losses greater than 10% (Table 6). The aesthetic aspect of brick with sludge was inspected after salt crystallisation test. Colorimetry results showed as bricks submitted to the salts crystallisation became darker, and the L^* parameter on dried samples decreased (L^* = 58.89) with respect to that of the same samples (brick 3) before the test (L^* = 71.95). Dried and wetted bricks after salt crystallisation displayed rather similar values (ΔE in Table 3), confirming little changes in the colour.

4. Conclusions

The characterization of the commercial bricks and the optimization of the new mix design obtained reusing a ceramic sludge confirms the close relationships between mineralogy, porosity, mechanical properties and durability under different environmental stresses [19,30–32]. Indeed, the three different types of brick, obtained from the same clay and fired at the same temperature (1050 °C) are very similar in the final properties, except for some characteristics conferred by the use of the sludge instead of the standard quartz sand for brick 3 and the dye addition to the brick 2. The overall study, demonstrated the possibility of using ceramic sludge in brick mixtures and highlighted changes in brick properties when manganese oxide is added as a dye. The brick with sludge (brick 3) differs from the others for its porosity and frost behaviour probably due to the different grain size and grain packing with respect to the brick obtained by using a standard temper. Colorimetric tests showed that bricks made with sludge have an aesthetic appearance similar to those of the commercial yellow bricks, that is, the colour of the former is compatible for feasible substitution. As regards water behaviour, the sludge-made brick has the best pore interconnections and slightly higher open porosity, confirmed by mercury intrusion analysis and nitrogen adsorption. Uniaxial compression tests showed very similar stress values (σ) for the commercial bricks, indicating that, despite the change in temper, mechanical properties were also maintained.

Instead, the addition of hausmannite ($Mn^{2+}Mn_2^{3+}O_4$) to the paste as a dye (brick 2) confers a different final aspect (grey, as attended) and causes an increase in mechanical strength: hausmannite does not only act as a dye, but also changes brick texture, increasing vitrification and improving mechanical properties. These overall good mechanical features were also confirmed by ultrasound tests.

Contrasting behaviour was found as regards the durability of bricks. Commercial bricks 1 and 2 were particularly susceptible to salt crystallisation, whereas the experimental sludge-made brick was weaker after freeze-thaw cycles. These differences were due to the different pore system of the three bricks and the aptitude of

salt and ice to crystallize within pores. The mechanism of ice and salt growth is similar and gives rise to a similar type of damage [33]. The nucleation rate of salt is higher in pores with diameters between 1 and 10 μm [34]. In pores of less 0.1 μm, salt requires a considerable degree of saturation to precipitate, whereas in pores of more than 10 μm, salt prevents the generation of sufficient pressure to damage the pore structure [35]. Porous materials with high porosity and smaller pores are more prone to decay; this is probably the reason why bricks 1 and 2 are the weakest to salts crystallisation [36]. The increase in pore size of brick 3, instead, should increase also the frost resistance [30]. The weakest response to frost of brick 3, with a greater number of pores with a radius larger than 0.1 μm and the highest micro-porosity, suggests that crystals can however efficiently grow inside the material, damaging it. This behaviour was observed by Ravaglioli [37] in roofing tiles, in which pores with size in the range between 0.25 and 1.4 μm suffer more the frost damages [38,39].

This evidence indicates that, although the brick with added sludge represents a valid substitute for commercial brick 1 (yellow) from many viewpoints, it may be susceptible if used in cold climates.

Our results confirm the possibility of economic and ecologic ways of improving the brick industry and developing new products with waste materials, and therefore reducing the need of georesources.

Acknowledgements

This study was funded by Research Group RNM179 of the *Junta de Andalucía* and by Research Project MAT2012-34473. The research benefited by funding from INPS – *Gestione Ex Inpdap (Direzione Regionale Veneto)*, which provided the PhD "Doctor J" Grant over the period 2013-2015. The authors are grateful to SanMarco-Terreal factory, in particular to Franco Favaro and Francesco Stangherlin, and to Gabriel Walton who revised the English text.

References

[1] M. Dondi, B. Fabbri, M. Marsigli, Rassegna delle esperienze di riciclaggio di scarti industriali e urbani nella produzione di laterizi, L'industria dei laterizi 51 (1998) 160–178.
[2] M. Dondi, M. Marsigli, B. Fabbri, Recycling of industrial and urban wastes in brick production – a review (Part I), Tile Brick Int. 13 (1997) 218–225.
[3] M. Dondi, M. Marsigli, B. Fabbri, Recycling of industrial and urban wastes in brick production – a review (Part 2), Tile Brick Int. 13 (1997) 302–309.
[4] I. Demir, Effect of organic residues addition on the technological properties of clay bricks, Waste Manage. 28 (2008) 622–627.
[5] S.P. Raut, R.V. Ralegaonkar, S.A. Mandavgane, Development of sustainable construction material using industrial and agricultural solid waste: a review of waste-create bricks, Constr. Build. Mater. 25 (2011) 4037–4042.
[6] L. Zhang, Production of bricks from waste materials – a review, Constr. Build. Mater. 47 (2013) 643–655.
[7] P. Muñoz Velasco, M.P. Morales Ortíz, M.A. Mendívil Giró, L. Muñoz Velasco, Fired clay bricks manufactured by adding wastes as sustainable construction material – a review, Constr. Build. Mater. 63 (2014) 97–107.
[8] S. Neves Monteiro, C.M. Fontes Vieira, On the production of fired clay bricks from waste materials: a critical update, Constr. Build. Mater. 68 (2014) 599–610.
[9] C. Bories, M.E. Borredon, E. Vedrenne, G. Vilarem, Development of eco-friendly porous fired clay bricks using pore-forming agents: a review, J. Environ. Manage. 143 (2014) 186–196.
[10] J. Sancho, B. Fernández, J. Ayala, P. García, J.C. Recio, C. Rodríguez, J.L. Bernardo, Method of obtaining electrolytic manganese from ferroalloy production waste, in: 1st Spanish National Conference on Advances in Materials Recycling and Eco-Energy, Madrid, 2009.
[11] V.D. Scott, G. Love, Quantitative Electron Probe Microanalysis, John Wiley and Sons, New York, 1983.
[12] G. Chen, J. Wang, The preparation of marine geological certified reference materials polymetallic nodule GSPN-1 and marine sediment GSMS-1 from the Central Pacific Ocean, Geostand. Geoanal. Res. 22 (1998) 119–125.
[13] UNI EN 13755, Natural stone test methods – determination of water absorption at atmospheric pressure, CNR-ICR, Rome, 2008.
[14] NORMAL 29/88, Misura dell'indice di asciugamento (drying index), CNR-ICR, Rome, 1988.
[15] UNI EN 1925, Natural stone test methods – determination of water absorption coefficient by capillarity, CNR-ICR, Rome, 2000.
[16] UNI EN 1926, Natural stone test methods – determination of uniaxial compressive strength, ICNR-ICR, Rome, 2007.
[17] UNI EN 12371, Natural stone test methods – determination of frost resistance, CNR-ICR, Rome, 2010.
[18] UNI EN 12370, Natural stone test methods – determination of resistance to salt crystallisation, CNR-ICR, Rome, 2001.
[19] G. Cultrone, E. Sebastián, K. Elert, M.J. de la Torre, O. Cazalla, C. Rodriguez-Navarro, Influence of mineralogy and firing temperature in the porosity of bricks, J. Eur. Ceram. Soc. 34 (2004) 547–564.
[20] A. Gualtieri, M. Bellotto, G. Artioli, M. Clark, Kinetic study of the kaolinite-mullite reaction sequence. Part II: Mullite formation, Phys. Chem. Miner. 22 (1995) 215–222.
[21] G. Cultrone, E. Sebastián, M.J. de la Torre, Mineralogical and physical behaviours of solid bricks with additives, Constr. Build. Mater. 19 (2005) 39–48.
[22] L. Maritan, L. Nodari, C. Mazzoli, A. Milano, U. Russo, Influence of firing conditions in ceramic products: experimental study on clay rich in organic matter, Appl. Clay Sci. 31 (2006) 1–15.
[23] P. Duminuco, B. Messiga, M.P. Riccardi, Firing process of natural clays. Some microtextures and related phase compositions, Termodinamica Acta 321 (1998) 185–190.
[24] M.P. Riccardi, B. Messiga, P. Duminuco, An approach to the dynamics of clay firing, Appl. Clay Sci. 15 (1999) 393–409.
[25] G. Cultrone, C. Rodriguez-Navarro, E.M. Sebastián, O. Cazalla, M.J. de la Torre, Carbonate and silicate phase reactions during ceramic firing, Eur. J. Mineral. 13 (2001) 621–634.
[26] P. Kemp, Chemismus Tunesischer Wasser Und Landklassifikation Der Steppenstzone Oglat Merteba in Sud-Tunisien, Dietrich Reimer, Berlin, 1985.
[27] K.S.W. Sing, D.H. Everett, R.A.W. Haul, L. Moscou, R.A. Pierotti, J. Rouquerol, T. Siemieniewska, Reporting physisorption data for gas/solid systems with special reference to the determination of surface area and porosity, Pure Appl. Chem., IUPAC 57 (4) (1985) 603–619.
[28] S. Storck, H. Bretinger, W.F. Maier, Characterization of micro- and mesoporous solids by physisorption methods and pore-size analysis, Appl. Catal. A 174 (1998) 137–146.
[29] G. Cultrone, E. Sebastián, Fly ash addition in clayey materials to improve the quality of solid bricks, Constr. Build. Mater. 23 (2009) 1178–1184.
[30] M. Dondi, M. Marsigli, I. Venturi, Microstructure and mechanical properties of clay bricks: comparison between fast firing and traditional firing, Br. Ceram. Trans. 98 (1999) 12–18.
[31] K. Elert, G. Cultrone, C. Navarro, E. Sebastián Pardo, Durability of bricks used in the conservation of historic buildings – influence of composition and microstructure, J. Cult. Heritage 4 (2003) 91–99.
[32] C. Coletti, G. Cultrone, L. Maritan, C. Mazzoli, How to face the new industrial challenge of compatible, sustainable brick production: study of various types of commercially available bricks, Appl. Clay Sci. 124–125 (2016) 219–226.
[33] G. Scherer, Crystallization in pores, Cem. Concr. Res. 29 (1999) 1347–1358.
[34] A. Arnold, K. Zehnder, Salt weathering on monuments, in: The Conservation of Monuments in the Mediterranean Basin: The influence of coastal environment and salt spray on limestone and marble, Proceedings of 1st International Symposium, 1990, 31–58.
[35] J. Martínez-Martínez, D. Benavente, M. Gomez-Heras, L. Marco-Castaño, M.Á. García-del-Cura, Non-linear decay of building stones during freeze–thaw weathering processes, Constr. Build. Mater. 38 (2013) 443–454.
[36] D. Benavente, L. Linares-Fernández, G. Cultrone, E. Sebastián, Influence of microstructure on the resistance to salt crystallisation damage in brick, Mater. Struct. 39 (2006) 105–113.
[37] A. Ravaglioli, Evaluation of the frost resistance of pressed ceramic product based on the dimensional distribution of pores, Trans. Br. Ceram. Soc. 75 (1976) 92–95.
[38] K. Ikeda, H.-S. Kim, K. Jaizu, A. Higashi, Influence of firing temperature on frost resistance of roofing tiles, J. Eur. Ceram. Soc. 24 (2004) 3671–3677.
[39] M.I. Sánchez de Rojas, F.P. Marín, M. Frías, E. Valenzuela, O. Rodríguez, Influence of freezing test methods, composition and microstructure on frost durability assessment of clay roofing tiles, Constr. Build. Mater. 25 (2011) 2888–2897.
[40] D.L. Whitney, B.W. Evans, Abbreviations for names of rock-forming minerals, Am. Mineral. 95 (2010) 185–187.